# Folding and Unfolding of Helix-Turn-Helix Motifs in the Gas Phase

Lloyd W. Zilch, David T. Kaleta, Motoya Kohtani, Ranjani Krishnan, and Martin F. Jarrold
Department of Chemistry, Indiana University, Bloomington, Indiana, USA

Ion mobility measurements and molecular dynamic simulations have been performed for a series of peptides designed to have helix-turn-helix motifs. For peptides with two helical sections linked by a short loop region: $AcA_{14}KG_3A_{14}K+2H^+$, $AcA_{14}KG_5A_{14}K+2H^+$, $AcA_{14}KG_7A_{14}K+2H^+$, and $AcA_{14}KSar_3A_{14}K+2H^+$ (Ac = acetyl, A = alanine, G = glycine, Sar = sarcosine and K = lysine); a coiled-coil geometry with two anti-parallel helices is the lowest energy conformation. The helices uncouple and the coiled-coil unfolds as the temperature is raised. Equilibrium constants determined as a function of temperature yield enthalpy and entropy changes for the unfolding of the coiled-coil. The enthalpy and entropy changes depend on the length and nature of the loop region. For a peptide with three helical sections: protonated $AcA_{14}KG_3A_{14}KG_3A_{14}K$; a coiled-coil bundle with three helices side-by-side is substantially less stable than a geometry with two helices in an antiparallel coiled-coil and the third helix collinear with one of the other two. (J Am Soc Mass Spectrom 2007, 18, 1239–1248) © 2007 American Society for Mass Spectrometry

The function and activity of a protein is controlled by its conformation. The conformation is determined by the protein's potential energy surface, which is in turn determined by the amino acid sequence. We often think of the structure of a folded protein in a hierarchical way starting with the secondary structure elements and how they aggregate into motifs. The motifs then provide the building blocks for the larger structures or domains which provide the protein with its three dimensional structure [1]. The process of protein folding often appears to follow a similar hierarchical pathway, where in many cases the secondary structure elements appear early along the folding pathway.

The helix-turn-helix is one of the simplest and most commonly occurring motifs in nature. It is found in a variety of situations, including the DNA binding [2] and calcium binding [3] motifs. Previously, we have reported preliminary studies of the peptide $AcA_{14}KG_3A_{14}K$ (G3) (Ac = acetyl, A = alanine, G = glycine, and K = lysine) that was designed to adopt a helix-turn-helix motif in the gas phase [4]. In the +2 charge state of this peptide, both lysines are protonated, and the $A_{14}K$ units are expected to be helical. The protonated lysine side-chain caps the C-terminus of the helix, and in this configuration, the charge interacts favorably with the helix dipole [5]. Isolated $AcA_{15}K+H^+$ helices are remarkably stable in the gas phase, and have been shown to remain intact to over 700 K. The two helices in the $AcA_{14}KG_3A_{14}K + 2H^+$ peptide are separated by a $G_3$ loop. Glycine was used to make the loop because it is a helix breaker, i.e., it has low propensity to form helices in solution [6] and in the gas phase [7, 8]. The $AcA_{14}KG_3A_{14}K + 2H^+$ peptide is thus expected to possess two main conformations, at low temperature a coiled-coil arrangement with the two helices aligned side-by-side, and at high temperature an unfolded conformation where the helices are uncoupled [4]. In the coiled-coil geometry the helices are aligned antiparallel. This permits favorable interactions between the helix dipoles, however, the antiparallel arrangement is less common in nature than the parallel coiled-coil [9].

In this paper, we report studies of several peptides with the helix-turn-helix motif. In particular, we focus on a series of peptides with turns or loop sections of different lengths and composition. In $AcA_{14}KSar_3A_{14}K$ (Sar3) sarcosine substitutes for the glycine loop in $AcA_{14}KG_3A_{14}K$. Sarcosine is a glycine derivative with a methyl group replacing a hydrogen atom on the amide nitrogen, so that this residue cannot form helical hydrogen bonds with the amide nitrogen. In $AcA_{14}KG_5A_{14}K$ (G5) and $AcA_{14}KG_7A_{14}K$ (G7) the length of the glycine loop is increased to five and seven residues respectively. Finally, $AcA_{14}KG_3A_{14}KG_3A_{14}K$ (3HG3) has three $A_{14}K$ helical segments separated by G3 loops. The question with this peptide is whether or not the third helix will fold into a three helix coiled-coil bundle. This

Address reprint requests to Dr. M. F. Jarrold, Department of Chemistry, Indiana University, 800 E. Kirkwood Ave., Bloomington, IN 47405-7102, USA. E-mail: mfj@indiana.edu

arrangement occurs naturally, for example, in the spectrin repeat [10].

The objective of these studies is to learn about the helix-turn-helix motif using simple model peptides in a solvent-free environment. There are two reasons why studies of unsolvated peptides are desirable. First, by removing the interactions with the solvent, the system becomes much simpler to model and understand; and second, the aqueous environment is not the only environment that is important from a biological point of view. Membrane proteins are a large class of proteins that are involved in transport, recognition, and ligand-receptor binding. A large portion of the surface of membrane proteins is shielded from water. Even globular proteins with hydrophilic surfaces have a hydrophobic core from which water is largely excluded and interactions occur in a water-free environment.

In the studies described here, ion mobility measurements [11, 12] in conjunction with molecular dynamics simulations are used to investigate the conformations of the helix-turn-helix peptides as a function of temperature. In the ion mobility measurements the ions move through a buffer gas under the influence of a weak electric field. How rapidly they travel depends on the average collision cross section: ions with unfolded structures have larger collision cross sections, and move through the buffer gas more slowly than ions with compact, roughly-spherical structures. Conformations are assigned by comparing the measured cross sections to average cross sections calculated for structures derived from molecular dynamics simulations. In the present work, the two main classes of conformations expected here (the coiled-coil with anti-parallel helices and the unfolded conformation where the helices are uncoupled) are easily distinguished on the basis of their mobilities.

## Experimental

Ion mobility measurements were performed as a function of temperature to obtain information about the conformations present for the G3, G5, G7, Sar3, and 3HG3 peptides. The experimental apparatus used for these studies has been described in detail previously [13, 14]. Briefly, peptide solutions were electrosprayed in air, and the ions enter the apparatus through a heated capillary interface. The ions pass through a differentially pumped region, through an RF hexapole ion guide, and they are then focused into the drift tube. The drift tube is operated with around 4 torr of helium buffer gas and with a drift voltage of 180 to 380 V. Under the conditions employed the mobilities remain in the low field regime [15] where the mobility is independent of the drift field, collisional heating is negligible, and the ions are not aligned in the drift field.

Two drift tubes were used to cover the temperature range examined here. The low temperature drift tube [12] is cooled by liquid nitrogen that flows through channels in the drift tube. The temperature is regulated

by microprocessor based temperature controllers that operate cryovalves that are fed from a liquid nitrogen tank. The high temperature drift tube is heated by Thermocoax heaters (Alpharette, GA) connected to a variable voltage transformers. The temperature is regulated using microprocessor based controllers.

Some of the ions that travel across the drift tube exit through a small aperture. These ions are focused into a quadrupole mass spectrometer set to transmit the ion of interest. Ions that are transmitted through the quadrupole are detected by an off-axis collision dynode and dual microchannel plates. Average collision cross sections are determined by using an electrostatic shutter at the entrance of the drift tube to admit short pulses of ions; the ion signal at the detector is then recorded with a multichannel scaler synchronized with the electrostatic shutter. Drift time distributions are obtained by correcting the measured arrival time distributions to account for the time that the ions spend traveling outside of the drift tube. The measured drift times are converted into collision cross sections using:

$$\Omega_{avg}^{1,1} = \frac{(18\pi)^{1/2}}{16}\left[\frac{1}{m} + \frac{1}{m_b}\right]^{1/2}\frac{ze}{(k_BT)^{1/2}}\frac{t_DE}{L_p}$$

[14] where m and $m_b$ are the masses of the ion and buffer gas, respectively, ze is the charge, $t_D$ is the drift time, E is the drift field, and $\rho$ is the buffer gas number density.

All peptides were synthesized using FastMoc chemistry on the Applied Biosystems Model 433A peptide synthesizer (Foster City, CA). Normal FastMoc procedures were used for G3, Sar3, G5, and G7. A special procedure was used for the synthesis of the peptide with three helices, 3HG3. N-[(Dimethylamino)-1H-1,2,3,-triazolo[4,5-b]pyridin-1-ylmethylene]-N-methylmethanaminium Hexafluorophosphate N-oxide (HATU) was used for activation, and 10% 1,8-diazabicyclo [5,4,0]-undec-7-ene, 10% piperidine in DMF was used for deprotection. This mixture was used to disrupt β-sheet formation on the HMP resin, which increasingly hinders coupling at longer polymer lengths. After cleavage with a 95% trifluoroacetic acid/5% water solution, the peptides were precipitated with diethyl ether, centrifuged, and lyophilized. The peptides were used unpurified, but MALDI-TOF was used to verify the product. Electrospray solution consisted of 2 mg of peptide and 1 mL of TFA with 0.1 mL water in all cases.

## Molecular Dynamics Simulations

Molecular dynamics (MD) simulations were performed to obtain low-energy conformations for comparison with the experimental results. The simulations were performed with the MACSIMUS suite of programs [16] using the CHARMM 21.3 parameter set. All the simulations shown herein were started with the $A_{14}K$ subunits as α-helices. Initial conformations for the loop
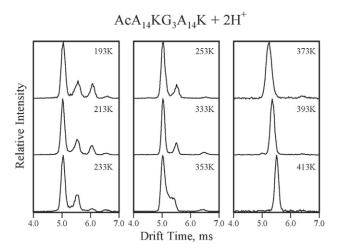
**Figure 1.** Representative drift time distributions recorded for the +2 charge state of the $AcA_{14}KG_3A_{14}K$ (G3) peptide as a function of temperature.

regions between the helical subunits were varied over a wide range. Simulations were done with a variety of simulated annealing schedules that were designed to prevent trapping in high-energy local minima. Three types of schedule, developed through trial and error, were used. A simple step-down cooling schedule that employed: 240 ps at 600 K, 240 ps at 500 K, 240 ps at 400 K, and 480 ps at 300 K. A step-up/step-down cooling schedule [17] that starts with 15 ps at 600 K followed by 45 ps at 590 K. The temperature is then stepped up by 200 K for 15 ps, and stepped down by 210 K for 45 ps. This step-up and step-down cycle is repeated until the temperature reaches 530 K. The temperature is then lowered to 300 K for 45 ps, raised to 500 K for 15 ps, and then terminates with 360 ps at 300 K. The total elapsed time is 915 ps. The third type of schedule employed here is a step-up/step-down heating schedule. Here the temperature starts at 200 K spikes to 400 K for 15 ps, then decreases to 210 K for 45 ps, spikes to 390 K for 15 ps, and so on, until the lower temperature reaches 300 K. This schedule was used to stabilize fragile conformations such as the coiled-coil bundle geometry for the triple helix peptide discussed below.

Average collision cross sections were calculated for conformations derived from the MD simulations using the empirically corrected exact hard sphere scattering approximation [18, 19], which correctly accounts for multiple scattering effects. Average cross sections were obtained by taking 50 snapshots from the last 35 ps of the MD simulation. The criterion for a match is that the calculated cross section is within 2% of the measured value.

## Results

Representative drift time distributions recorded for the +2 charge state of the $AcA_{14}KG_3A_{14}K$ (G3) peptide are shown in Figure 1. The drift time distributions for G3 show three distinct peaks at low temperatures (<250 K)

(the small peak at a drift time of around 6.5 ms is an artifact). Cross sections for the main features observed in the drift time distributions are plotted against temperature in Figure 2. The points show the experimental results while the lines show empirical fits to the cross sections using a simple exponential function. If the structure remains unchanged as the temperature is raised, the cross sections systematically decrease because the long range interactions between the ion and the buffer gas become less important.

Figure 3 shows the results of the MD simulations for the G3 peptide. This figure shows a plot of the average energy versus average cross section from the last 35 ps of each simulation. The simulations all terminate at 300 K. The vertical lines in Figure 3 show the cross sections for the three features found in the experiments (extrapolated to 300 K where necessary). A close grouping of points in Figure 3 represents a favored structure. The lowest energy grouping with cross sections around 460 $Å^2$ is due to the coiled-coil structure. A representative snap shot taken from the MD simulations for this group is shown in the figure. The average cross sections for this group are close (<2% difference) to the value for the peak with the shortest drift time (smallest cross section) in the experimental results, and so this peak is assigned to the coiled-coil geometry. There is a second group of coiled-coil geometries at a slightly higher energy and slightly larger cross section (see Figure 3). It is likely that these structures also contribute to the average conformation sampled in the experiments. The other main low-energy group in Figure 3 occurs at cross sections around 540 $Å^2$. These structures have the helices uncoupled. The lowest energy geometries for
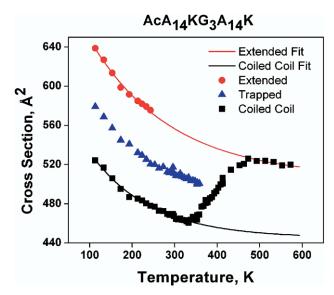


**Figure 2.** Plot of the cross sections for the main features found in the drift time distributions for the +2 charge state of the $AcA_{14}KG_3A_{14}K$ (G3) peptide as a function of temperature. The points show the measured cross sections and the lines are empirical fits using a simple exponential function. The labels extended, trapped, and coiled-coil refer to the structural assignments described in the text.

**Figure 3.** Plot of average energy against average cross section from the last 35 ps of the MD simulations for the +2 charge state of the $AcA_{14}KG_3A_{14}K$ (G3) peptide. The simulations all terminate at 300 K. The vertical lines show the cross sections for the three features found in the experiments (extrapolated to 300 K where necessary).

this motif have nearly collinear helices as shown in Figure 3. The average cross section for this group is slightly smaller (~3%) than the value for the peak with the longest drift time (largest cross section). However, there is no other viable alternative, so we assign this peak to the extended or uncoupled geometry. There is no low-energy group with cross sections close to the value for the peak with the intermediate drift times. While there are some low-energy points with cross sections close to the value for the middle peak, further inspection of the simulations leading to these values suggests that these are due to transients where the structure is changing between the extended and the coiled-coil conformations. The most likely assignment for the middle feature is a high-energy malformed structure with exchanged lysines (see Figure 3). This motif yields a small group of points that are around 100 kJ mol$^{-1}$ above the lowest energy coiled-coil motif. Further support for this motif being responsible for the middle peak in the drift time distributions will be described below.

We return now to consider the temperature dependence of the drift time distributions for G3 (see Figures 1 and 2). As the temperature is raised above 250 K the peak due to the extended conformation disappears, and then at around 350 K the peak assigned to the misfolded conformation disappears leaving behind the peak assigned to the coiled-coil. The disappearance of the peak attributed to the metastable structure clearly occurs under kinetic control. At low temperature the metastable structure is trapped. But as the temperature is raised it converts into the coiled-coil on the timescale of the drift time measurements. The signature of this behavior is the formation of a bridge between the peaks in the drift time distribution. The bridge results from peptide ions that spend part of their time in the metastable structure and part in the coiled-coil, so that the average drift time lies between the two peaks. A bridge is clearly evident in the drift time distributions recorded for G3 at 353 K (see Figure 1). Note that the metastable malformed structure is not an intermediate along the potential energy surface between the coiled-coil and unfolded conformations, even though the cross sections for the malformed structure lie between those for the coiled-coil and unfolded conformations.

For temperatures above 350 K, the measured cross sections begin to diverge from the line predicted for the coiled-coil, and rise to the level expected for the unfolded conformation by around 450 K (see Figure 2). Within this 350 to 450 K temperature range, the peak in the drift time distributions moves gradually from the position expected for the coiled-coil to that expected for the unfolded conformation. This is the signature of a transition occurring under equilibrium control where the rate of interconversion between the two conformations is fast compared to the time spent traveling across
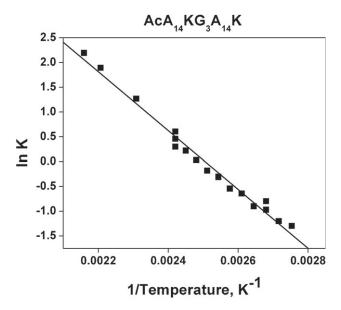
**Figure 4.** Plot of $ln$K against $1/T$ for uncoupling of the helices in the +2 charge state of the $AcA_{14}KG_3A_{14}K$ (G3) peptide. The points are the results and the line is a least-squares fit.

the drift tube. Assuming that we are dealing with a two state system where the ions spend the vast majority of their time in either the coiled-coil or the unfolded conformation, then the position of the measured cross section relative to the cross sections for the coiled-coil and unfolded conformations is a measure of the amount of time spent in each conformation. When the measured cross section is close to the value expected for the coiled-coil, the peptide spends most of its time as a coiled-coil, and when the cross section is close to that expected for the unfolded conformation, it spends most of its time unfolded. The time spent in each conformation is related to the equilibrium constant, and a value for the equilibrium constant can be obtained from:

$$K = \frac{\sigma_{measured} - \sigma_{coiled-coil}}{\sigma_{unfolded} - \sigma_{measured}}$$

where $\sigma_{measured}$ is the measured cross section, and $\sigma_{coiled-coil}$ and $\sigma_{unfolded}$ are the cross sections expected for the coiled-coil and unfolded conformations. A plot of $ln$K against $1/T$ for uncoupling of the helices in the +2 charge state of the $AcA_{14}KG_3A_{14}K$ (G3) peptide is shown in Figure 4. The slope of the line in this plot is the enthalpy change for the uncoupling of the helices and the intercept is the entropy change. The line in Figure 4 shows a linear least-squares fit from which the following values are obtained: $\Delta H^o = 49 \pm 2$ kJ mol$^{-1}$ and $\Delta S^o = 124 \pm 4$ J K$^{-1}$ mol$^{-1}$. These results differ slightly from the preliminary results reported in Ref. 4 ($\Delta H^o = 45 \pm 2$ kJ mol$^{-1}$ and $\Delta S^o = 115 \pm 5$ J K$^{-1}$ mol$^{-1}$). The equilibrium constants reported here were obtained over a significantly broader temperature range.

Figure 5 shows a plot of the cross sections for the

main features observed in the drift time distributions for the +2 charge state of the $AcA_{14}KSar_3A_{14}K$ (Sar3) peptide. The main difference between the results for G3 and Sar3 is that the feature assigned to the misfolded conformation for the G3 peptide is absent for Sar3. The MD simulations for Sar3 show prominent groups due to the coiled-coil and unfolded motifs. However, the misfolded conformation which forms for the G3 peptide at high temperatures during simulated annealing did not form for the Sar3 peptide. We forced the Sar3 peptide into the misfolded conformation (with exchanged lysines) but it quickly annealed away at a relatively low temperature. So apparently this conformation is not metastable for the Sar3 peptide. We believe that this provides further support for the assignment of this feature for G3 to the misfolded structure with exchanged lysines. Substitution of glycine (G3) by sarcosine (Sar3) evidently destabilizes the misfolded conformation, perhaps by limiting the conformational freedom required to adopt this motif.

The Sar3 peptide undergoes a transition between 400 and 500 K similar to that found at elevated temperatures for G3. The cross sections move from the position expected for the coiled-coil motif to that expected for the unfolded conformation, as this occurs the peak in the drift time distribution moves smoothly and remains narrow, indicating that the transition occurs under equilibrium control. Equilibrium constants were derived from the cross sections in the transition region using the approach described above. Figure 6 shows a plot of $ln$K against $1/T$ for Sar3. The points are the experimental results and the line is a linear least-squares fit, from which the following values were
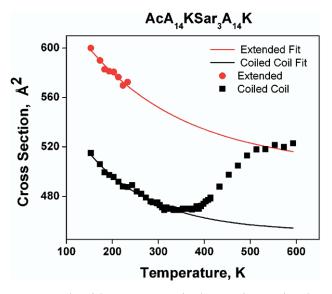


**Figure 5.** Plot of the cross sections for the main features found in the drift time distributions for the +2 charge state of the $AcA_{14}KSar_3A_{14}K$ (Sar3) peptide as a function of temperature. Two peaks are found in the drift time distributions at low temperature, which are assigned to the coiled-coil structure (with the smaller cross sections) and an extended structure (with the larger cross sections).
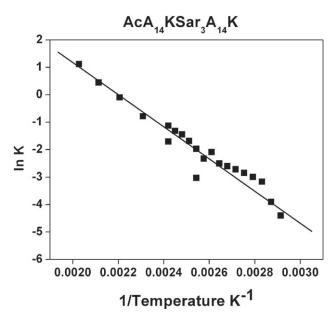
**Figure 6.** Plot of *ln*K against 1/T for uncoupling of the helices in the +2 charge state of the $AcA_{14}KSar_3A_{14}K$ (Sar3) peptide. The points are the results and the line is a least-squares fit.
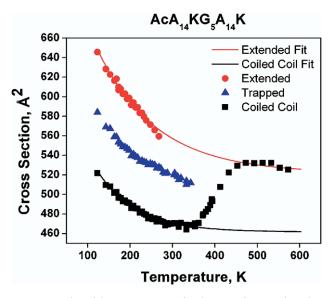


**Figure 7.** Plot of the cross sections for the main features found in the drift time distributions for the +2 charge state of the $AcA_{14}KG_5A_{14}K$ (G5) peptide as a function of temperature. Three peaks are found in the drift time distributions at low temperature, which are assigned to the coiled-coil structure (which has the smallest cross sections), a misfolded structure (which has the intermediate cross sections) and an extended structure (with the largest cross sections).

deduced: $\Delta H° = 43 \pm 3$ kJ mol$^{-1}$ and $\Delta S° = 93 \pm 8$ J K$^{-1}$ mol$^{-1}$. These values are compared to analogous ones for G3 in Table 1.

Three conformations are observed for the $AcA_{14}KG_5A_{14}K+2H^+$ (G5) peptide at low temperatures. A plot of the cross sections against temperature for the G5 peptide is shown in Figure 7. The results are similar to those for the G3 peptide, and the three conformations observed at low temperature for G5 are assigned to a coiled-coil, misfolded, and extended conformations, in order of increasing cross section. As the temperature is raised the extended conformation disappears first, followed by the misfolded at around 350 K. Then as the temperature is raised further the helices in the coiled-coil arrangement become uncoupled. Equilibrium constants were obtained in the transition region. The plot of *ln*K against 1/T for G5 is linear, and a least-squares fit yields $\Delta H° = 62 \pm 4$ kJ mol$^{-1}$ and $\Delta S° = 154 \pm 9$ J K$^{-1}$ mol$^{-1}$. These values are compared to analogous ones for G3 and Sar3 in Table 1. The results for the $AcA_{14}KG_7A_{14}K+2H^+$ (G7) peptide are similar to those for G5. The following values were derived for G7 from the plot of *ln*K against 1/T: $\Delta H° = 56 \pm 2$ kJ mol$^{-1}$ and $\Delta S° = 158 \pm 5$ J K$^{-1}$ mol$^{-1}$.

For the $AcA_{14}KG_3A_{14}KG_3A_{14}K$ (3HG3) peptide,

which is three helical sections, the +2 charge state is more abundant than the +3. Ion mobility measurements were performed for both the +2 and +3 charge states. Cross sections for the main features observed in the drift time distributions are plotted against temperature in Figure 8. One main feature is observed for the +3 charge state. For the + 2 charge state, three features are observed that appear to parallel the features found for G3, G5, and G7. Figure 9 shows a plot of the average energy against the average cross section (at 300 K) for the last 35 ps of the MD simulations for the +3 charge state of $AcA_{14}KG_3A_{14}KG_3A_{14}K$. The vertical dashed lines in Figure 9 show the cross sections, at 300 K, for the three main features observed for the +2 charge state of 3HG3. The two larger cross sections were extrapolated using the empirical fits shown in Figure 8. The cross section for the feature observed for the +3 charge state of 3HG3 is almost identical to the smallest cross section for the +2 charge state. The points shown in Figure 9 have been grouped into motifs by inspection. The observed conformations were found to fall into four main groups. Representative snap shots for the

**Table 1.** Summary of enthalpy and entropy changes for the transitions between the coiled-coil and the extended conformation with uncoupled helices

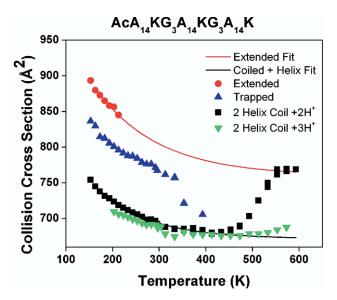| Peptide | $\Delta H°$, kJ mol$^{-1}$ | $\Delta S°$, J K$^{-1}$ mol$^{-1}$ |
|---|---|---|
| $AcA_{14}KG_3A_{14}K + 2H^+$ (G3) | $49 \pm 2$ | $124 \pm 4$ |
| $AcA_{14}KSar_3A_{14}K + 2H^+$ (Sar3) | $43 \pm 3$ | $93 \pm 8$ |
| $AcA_{14}KG_5A_{14}K + 2H^+$ (G5) | $62 \pm 4$ | $154 \pm 9$ |
| $AcA_{14}KG_7A_{14}K + 2H^+$ (G7) | $56 \pm 2$ | $158 \pm 5$ |
| $AcA_{14}KG_3A_{14}KG_3A_{14}K + 2H^+$ (3HG3) | $98 \pm 5$ | $193 \pm 9$ |

**Figure 8.** Plot of the cross sections for the main features found in the drift time distributions for the +2 and +3 charge states of the AcA$_{14}$KG$_3$A$_{14}$KG$_3$A$_{14}$K (3HG3) peptide as a function of temperature. For the +2 charge state, three peaks are found in the drift time distributions at low temperature, which are assigned to the coiled-coil helix structure (which has the smallest cross sections), a trapped T-shaped structure, and an extended structure (with the largest cross sections). For the +3 charge state only one main feature is observed which is assigned to a coiled-coil helix structure. See text for an explanation of the structural assignments.

four motifs are shown in Figure 10. The lowest energy motif, represented by the red circles in Figure 9, consists of two helices in a coiled-coil arrangement and one helix uncoupled from the other two. An example of this structure is shown in Figure 10b. The cross sections for the coiled-coil helix motif matches the cross section for the feature observed for the +3 charge state, and the feature with the smallest cross section found for the +2 charge state. The next lowest energy motif evident in Figure 9 is the extended structure with completely uncoupled helices. An example of this motif is shown in Figure 10a. The points for this motif are the black squares in Figure 9, and we assign the feature with the largest cross section in the measurements for the +2 charge state to this motif. The green inverted triangles in Figure 9 are due to a bent T-shaped structure like that shown in Figure 10c. The cross sections for this motif match the intermediate cross sections found for the +2 charge state. The coiled-coil bundle shown in Figure 10d, and represented by the blue triangles in Figure 9, does not appear to be present in the experiments. This motif, which has all three helices in a coiled-coil arrangement, has an average cross section that is substantially smaller than any feature observed in the experiments for the 3HG3 peptide. It is evident from Figure 9 that the coiled-coil bundle is a relatively high-energy conformation, it appears to be around 150 kJ mol$^{-1}$ higher in energy than the lowest energy coiled-coil helix arrangement (which has two parallel helices). The coiled-coil bundle did not form spontaneously in the

simulations. The blue triangles in Figure 9 were all started from a conformation forced into an arrangement with three parallel helices. The coiled-coil bundle is not very stable and readily opens up to the lower-energy coiled-coil helix arrangement.

As the temperature is raised, some of the features that are present at low temperature for 3HG3 disappear (see Figure 8). First the feature assigned to the extended motif disappears at around 220 K, and then middle feature assigned to the trapped T-shaped conformation disappears between 300 and 400 K. Finally, as the temperature is raised further, the helices in the coiled-coil helix conformation uncouple to give the fully extended conformation. The uncoupling occurs under equilibrium control, and Figure 11 shows a plot of $ln$K against 1/T for this process. The following values were derived from the linear least-squares fit shown in the figure: $\Delta H^o = 98 \pm 5$ kJ mol$^{-1}$ and $\Delta S^o = 193 \pm 9$ J K$^{-1}$ mol$^{-1}$. These values are compared in Table 1 to the other values obtained from this work. The coiled-coil helix conformation for the +3 charge state only appears to partly uncouple over the temperature range examined here.

## Discussion

The two main conformations that are important for peptides with a helix-coil-helix motif are the coiled-coil arrangement with antiparallel helices and the extended conformation with uncoupled helices. In addition, there is also a metastable, misfolded conformation with exchanged lysines that is important for G3, G5, and G7. The misfolded structure may become trapped during the electrospray process or form during the collisional heating that occurs as the ions enter the drift tube. Once
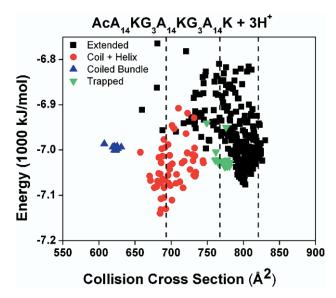


**Figure 9.** Plot of average energy against average cross section for the last 35 ps of the MD simulations for the +3 charge state of the AcA$_{14}$KG$_3$A$_{14}$KG$_3$A$_{14}$K (3HG3) peptide. The different shapes and colors represent different motifs that are discussed in the text.
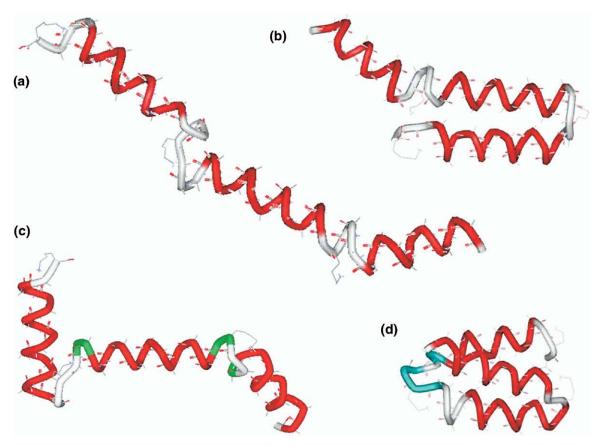
**Figure 10.** Representative snapshots taken from the MD simulations for the +3 charge state of the AcA$_{14}$KG$_3$A$_{14}$KG$_3$A$_{14}$K (3HG3) peptide. (**a**) is an example of an extended conformation with uncoupled helices; (**b**) is an example of a coiled-coil helix conformation; (**c**) is an example of a trapped T-shaped conformation; and (**d**) is an example of a coiled-coil bundle.

formed, the metastable structure is trapped in a local energy minimum and more energy is required to disrupt the exchanged lysine arrangement. For the Sar3 peptide, however, the local energy minimum appears to be much shallower, and the metastable conformation is not observed for Sar3.

A transition between the coiled-coil and the extended conformation occurs under thermodynamic control as the temperature is raised. For G3, G5, G7, and Sar3 the transition occurs at around 350 to 450 K. The enthalpy changes deduced from these studies provide a measure of the strength of the interactions holding the helices in the coiled-coil arrangement. G5 and G7 probably provide the best measure of this quantity because the loops are long enough in these peptides to allow the helices to interact in their optimum relative orientations. Based on G5 and G7, the strength of the interactions between the A$_{14}$K helices in the coiled-coil geometry is around 60 kJ mol$^{-1}$. There are no specific interactions between the polyalanine based helices and so the interactions that are present are due to van der Waals interactions and interactions between the helix macro-dipoles. The helix macro-dipoles are orientated antiparallel to each other which results in favorable interactions. The enthalpy change for G3 is smaller than
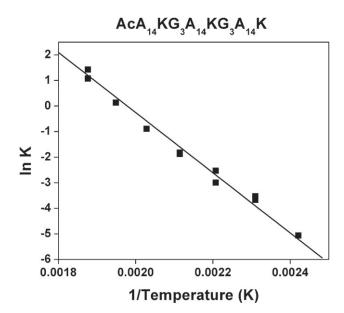


**Figure 11.** Plot of $ln$K against $1/T$ for uncoupling of the helices in the +2 charge state of the AcA$_{14}$KG$_3$A$_{14}$KG$_3$A$_{14}$K (3HG3) peptide. The points are the results and the line is a least-squares fit.

for G5 and G7, probably because the G3 loop is not long enough for the helices to find their optimum relative orientations. The enthalpy change for Sar3 is smaller than for G3 presumably for the same reason, a sarcosine loop is more constrained than a glycine loop. The enthalpy change for G3, 49 kJ mol$^{-1}$, can be compared to the energy difference between the coiled-coil and extended conformations in the MD simulations for G3. From the results shown in Figure 3 the energy difference between the lowest energy coiled-coil and extended conformation is around 25 kJ mol$^{-1}$. A factor that may contribute to this difference being smaller than the measured enthalpy change is that the energy difference is taken at 300 K where the loop region of the extended conformation may still be partially ordered.

The uncoupling of the helices that occurs as the temperature is raised is driven by entropy. When the helices become uncoupled the loop region is able to access more conformations. The backbone entropy of glycine has been estimated to be around 28 J K$^{-1}$ mol$^{-1}$ [20]. So if the glycines in the G3 loop region are completely constrained in the coiled-coil geometry and completely free in the extended conformation, the entropy change should be $\Delta S^o = 3 \times 28$ J K$^{-1}$ mol$^{-1}$ = 84 J K$^{-1}$ mol$^{-1}$. This is somewhat smaller than the measured value of 124 J K$^{-1}$ mol$^{-1}$. This discrepancy may result from fraying of the helices at the point where the glycine loop joins the helix. The measured entropy change for Sar3 (93 J K$^{-1}$ mol$^{-1}$) is smaller than for G3 which is expected because the backbone entropy of sarcosine is smaller than for glycine. The entropy changes increase along the series G3, G5, and G7 (124, 154, and 158 J K$^{-1}$ mol$^{-1}$). However, the difference between the entropy changes is significantly less than twice the backbone entropy of glycine (56 J K$^{-1}$ mol$^{-1}$). As the glycine loop becomes longer it becomes more flexible in the coiled-coil conformation, and so the increment in the entropy change that occurs when the helices uncouple should become smaller (as observed).

Only a single feature is observed for the +3 charge state of the AcA$_{14}$KG$_3$A$_{14}$KG$_3$A$_{14}$K (3HG3) peptide which corresponds to a structure with two helices in a coiled-coil arrangement while the other helix is uncoupled. This is the lowest energy motif found in the MD simulations for 3HG3. The motif with three helices in a coiled-coil bundle is not observed in the experiments. According to the MD simulations the coiled-coil bundle is around 150 kJ mol$^{-1}$ less stable than the coiled-coil helix geometry. One possible reason why it is not energetically favorable to fold the third helix into a coiled-coil bundle is that the G3 loop regions are too short for the peptide to adopt a favorable arrangement of the three helices. We explored this by doing some simulations for peptides with longer loop regions and concluded that while the G3 loop maybe slightly shorter than optimum, this is not the main reason why it is energetically unfavorable to make the coiled-coil bundle. The main reason appears to be the interactions between the helix macro-dipoles. When the first two

helices are aligned antiparallel to each other the helix macro-dipoles interact favorably. However, when the third helix is brought in, the interaction is less favorable because this helix must be parallel to one of the other two helices. In a parallel arrangement the interaction between the helix macro-dipoles is unfavorable.

As the temperature is raised, the +3 charge state of the AcA$_{14}$KG$_3$A$_{14}$KG$_3$A$_{14}$K peptide (3HG3 + 3H$^+$) remains in the coiled-coil helix motif. The helices for this peptide apparently do not uncouple, at least not over the temperature range examined here. There is some indication that the cross sections for the 3HG3 + 3H$^+$ peptide start to diverge from the line for the coiled-coil helix for temperatures above 500 K (see Figure 8). This may indicate the beginning of an uncoupling transition but clearly this process occurs at a much higher temperature than for G3, G5, G7, and Sar3. One factor that may contribute to the additional stabilization of the coiled-coil helix motif for the 3HG3 + 3H$^+$ peptide is revealed in Figure 10b which shows a snap shot for this motif taken from the simulations. In the center, there are two protonated lysine groups, one attached to the dangling helix, and the other attached to the lower helix in the coiled-coil. The lysine attached to the dangling helix also appears to be associated with the end of the helix in the coiled-coil, essentially forming a bridge across the end of the coiled-coil. This interaction clearly helps to resist the opening-up of the coiled-coil, and thus presumably contributes to the additional stabilization of the coiled-coil helix geometry for the 3HG3 + 3H$^+$ peptide. The arrangement of the charges evident in Figure 10b results in two positive charges in quite close proximity. This type of arrangement has been seen before [21, 22] and is attributed to cooperative stabilization: bringing the positive charges together in this way allows both of them to interact with the macro-dipoles of both helices. The other possible way of arranging the helices and charges in the coiled-coil helix geometry is to have a protonated lysine at the end of the dangling helix, and the other two at each end of the coiled-coil. This arrangement avoids having two protonated lysine groups in close proximity as in Figure 10c but overall it appears to be less favorable in the simulations, presumably because of the cooperative stabilization mentioned above.

For the +2 charge state of the 3HG3 peptide, the helices in the coiled-coil helix motif uncouple as the temperature is raised. However, the enthalpy and entropy changes ($\Delta H^o = 98$ kJ mol$^{-1}$ and $\Delta S^o = 193$ J K$^{-1}$ mol$^{-1}$) are substantially larger than for the analogous G3 peptide that has only two helical sections and a single G3 loop ($\Delta H^o = 49$ kJ mol$^{-1}$ and $\Delta S^o = 124$ J K$^{-1}$ mol$^{-1}$). The substantial increase in the entropy change on going from G3 to 3HG3 + 2H$^+$ suggests that both the G3 loop regions are constrained in the 3HG3 + 2H$^+$ peptide at low temperature. In Figure 10b the loop region between the dangling helix and the first helix in the coiled-coil is in a helical conformation, so that the N-terminus AcA$_{14}$KG$_3$A$_{14}$K- unit forms an extended

helix at low temperature. This is probably because the protonated lysine that should be associated with the dangling helix is interacting instead with the second helix in the coiled-coil.

While the enthalpy change for 3HG3 + 2H$^+$ is larger than for the G3 peptide, it is smaller than for 3HG3 + 3H$^+$. Above we attributed the high stability of the coiled-coil helix geometry in the 3HG3 + 3H$^+$ peptide to cooperative stabilization involving the two protonated lysines in the center of the peptide. If one of these protons is removed to generate the +2 charge state of the 3HG3 peptide, this will weaken the cooperative stabilization so that the coiled-coil opens up at a lower temperature for the +2 charge state of 3HG3 than for the +3 charge state. However, the single protonated lysine in the central position still stabilizes the coiled-coil geometry with respect to the G3 peptide.

## Acknowledgments

## References

1. Branden, C.; Tooze, J. *Introduction to Protein Structure*, 2nd ed.; Garland: New York, 1999, pp.13–30.
2. Anderson, W. F.; Ohlendorf, W. H.; Takeda, Y.; Matthews, B. W. Structure of the Cro Repressor from Bacteriophage and its Interaction with DNA. *Nature* **1981,** *290,* 754–758.
3. Kretsinger, R. H.; Nockolds, C. E. Carp Muscle Calcium Binding Protein. 2. Structure Determination and General Description. *J. Biol. Chem.* **1973,** *248,* 3313–3326.
4. Kaleta, D. T.; Jarrold, M. F. Helix-Turn-Helix Motifs in Unsolvated Peptides. *J. Am. Chem. Soc.* **2003,** *125,* 7186–7187.
5. Hudgins, R. R.; Ratner, M. A.; Jarrold, M. F. Design of Helices that are Stable in vacuo. *J. Am. Chem. Soc.* **1998,** *120,* 12974–12975.
6. Chakrabartty, A.; Baldwin, R. L. Stability of α-Helices. *Adv. Protein Chem.* **1995,** *46,* 141–176.
7. Hudgins, R. R.; Mao, Y.; Ratner, M. A.; Jarrold, M. F. Conformations of Gly$_n$H$^+$ and Ala$_n$H$^+$ Peptides in the Gas Phase. *Biophys. J.* **1999,** *76,* 1591–1597.
8. Hudgins, R. R.; Jarrold, M. F. Conformations of Unsolvated Glycine-Based Peptides. *J. Phys. Chem. B.* **2000,** *104,* 2154–2158.
9. Oakley, M. G.; Hollenbeck, J. J. The Design of Antiparallel Coiled-Coils. *Curr. Opin. Struct. Biol.* **2001,** *11,* 450–457.
10. Yan, Y.; Winograd, E.; Viel, A.; Cronin, T.; Harrison, S. C.; Branton, D. Crystal Structure of the Repetitive Segments of Spectrin. *Science* **1993,** *262,* 2027–2030.
11. Clemmer, D. E.; Jarrold, M. F. Ion Mobility Measurements and their Applications to Clusters and Biomolecules. *J. Mass Spectrom.* **1997,** *32,* 577–592.
12. Wyttenbach, T.; Bowers, M. T. Gas-Phase Conformations: The Ion Mobility/Ion Chromatography Method. *Top. Curr. Chem.* **2003,** *225,* 207–232.
13. Kinnear, B. S.; Hartings, M. R.; Jarrold, M. F. Helix Unfolding in Unsolvated Peptides. *J. Am. Chem. Soc.* **2001,** *123,* 5660–5667.
14. Kohtani, M.; Jones, T. C.; Schneider, J. E.; Jarrold, M. F. Extreme Stability of an Unsolvated α-Helix. *J. Am. Chem. Soc.* **2004,** *126,* 7420–7421.
15. Mason, E. A.; McDaniel, E. W. Transport Properties of Ions in Gases; Wiley: New York, 1988, pp. 150–156.
16. http://www.icpf.cas.cz/jiri/macsimus/default.htm
17. Kohtani, M.; Jarrold, M. F. The Initial Steps in the Hydration of Unsolvated Peptides: Water Molecule Adsorption on Alanine-Based Helices and Globules. *J. Am. Chem. Soc.* **2002,** *124,* 11148–11158.
18. Kinnear, B. S.; Kaleta, D. T.; Kohtani, M.; Hudgins, R. R.; Jarrold, M. F. Conformations of Unsolvated Valine-Based Peptides. *J. Am. Chem. Soc.* **2000,** *122,* 9243–9256.
19. Shvartsburg, A. A.; Jarrold, M. F. An Exact Hard-Spheres Scattering Model for the Mobilities of Polyatomic Ions. *Chem. Phys. Lett.* **1996,** *261,* 86–91.
20. Zhang, C.; Cornette, J. L.; Delisi, C. Consistency in Structural Energetics of Protein Folding and Peptide Recognition, *Prot. Sci.* **1997,** *6,* 1057–1064.
21. Kaleta, D. T.; Jarrold, M. F. Peptide Pinwheels. *J. Am. Chem. Soc.* **2002,** *124,* 1154–1155.
22. Kaleta, D. T.; Jarrold, M. F. Noncovalent Interactions between Unsolvated Peptides. *J. Phys. Chem. A* **2002,** *106,* 9655–9664.